Enhanced and tunable surface plasmons in two-dimensional Ti_3C_2 stacks: Electronic structure versus boundary effects

Vincent Mauchamp,[1,*] Matthieu Bugnet,[2] Edson P. Bellido,[2] Gianluigi A. Botton,[2] Philippe Moreau,[3] Damien Magne,[1] Michael Naguib,[4] Thierry Cabioc'h,[1] and Michel W. Barsoum[4]

[1]*Institut Pprime, UPR 3346 CNRS-Université de Poitiers-ISAE-ENSMA, Boîte Postale 30179, 86962 Futuroscope-Chasseneuil Cedex, France*

[2]*Department of Materials Science and Engineering, McMaster University, 1280 Main Street West, Hamilton, Ontario L8S 4M1,Canada*

[3]*Institut des Matériaux Jean Rouxel (IMN), Université de Nantes, CNRS, 2 rue de la Houssinière, Boîte Postale 32229, 44322 Nantes Cedex 3, France*

[4]*Department of Materials Science and Engineering, Drexel University, Philadelphia, Pennsylvania 19104, USA*

(Received 12 December 2013; revised manuscript received 9 May 2014; published 20 June 2014)

The dielectric response of two-dimensional (2D) Ti_3C_2 stacked sheets was investigated by high-resolution transmission electron energy-loss spectroscopy and *ab initio* calculations in the 0.2–30-eV energy range. Intense surface plasmons (SPs), evidenced at the nanometer scale at energies as low as 0.3 eV, are shown to be the dominant screening process up to at least 45-nm-thick stacks. This domination results from a combination of efficient free-electron dynamics, begrenzungs effect, and reduced interband damping. It is shown that, in principle, the SPs energies can be tuned in the mid-infrared, from 0.2 to 0.7 eV, by controlling the sheets' functionalization and/or thickness. This point evidences a new attribute of this new class of 2D materials.

DOI: 10.1103/PhysRevB.89.235428 PACS number(s): 78.66.−w, 73.20.Mf, 78.67.Pt, 79.20.Uv

I. INTRODUCTION

Two-dimensional (2D) materials offer a large playground in condensed-matter physics, graphene [1] being the most popular of these systems among others, such as hexagonal boron nitrides (h-BNs) or transition-metal dichalcogenides (TMDs) [2,3]. Because of their high aspect ratio, these systems exhibit outstanding surface properties which perfectly match the growing field of plasmonics, i.e., the manipulation of light at subwavelength scales through its coupling with surface plasmons (SPs) [4]. In such systems, the confinement of the electromagnetic field at the surface leads to many applications related to surface-enhanced optical phenomena [5], which in the mid-infrared, are of particular interest for chemical sensing, thermal imaging, or photovoltaic applications [6]. Although graphene is very promising from this point of view since its SP characteristics can be tuned electrically, by chemical doping or nanostructuration [7,8], the recent discovery of a new class of 2D crystals, called MXenes [9,10], brings new possibilities in the investigation of 2D crystals and their applications for plasmonics.

MXenes are 2D early transition-metal (M) carbides and/or carbonitrides stacked sheets of various thicknesses [see the inset of Fig. 1(b)]. These sheets are obtained by chemical etching of the A element (mostly elements from groups III-A or IV-A) from the $M_{n+1}AX_n$ phases, the latter being layered ternary carbides or nitrides (X = C or N) [11]. The $M_{n+1}AX_n$ phases are composed of stacks of $M_{n+1}X_n$ octahedra layers interleaved with layers of a pure A element with many possible chemical substitutions on each of the three, viz. M, A, or X, sites. MXenes are thus a potentially large family of 2D $M_{n+1}X_n$ weakly interacting layers. Because of the chemical treatment leading to their formation, the $M_{n+1}X_n$ layers are passivated with OH and/or F terminations [10]. Discovered very recently, these materials have already been intensively investigated both experimentally and theoretically [12–15]. In particular, MXenes exhibit outstanding properties in terms of intercalation applications [16,17], and are interesting for optoelectronic devices since they combine optical transparency and metallic character [10,18].

In the present study, we highlight the connection between the dielectric response and the nanostructuration of one of the most studied MXenes to date, namely $Ti_3C_2T_2$ (T = OH or F), and evidence the properties of its mid-infrared SPs. The dielectric properties, including bulk and surface modes, have been characterized using high-resolution electron energy-loss spectroscopy (HREELS) performed in a monochromated scanning transmission electron microscope (STEM), which is an invaluable tool for such investigations at the nanometer scale [19,20]. Using a complete *ab initio* theoretical framework for the interpretation of our data, we show that: (i) $Ti_3C_2T_2$ exhibits intense SPs that can be detected at the nanometer scale at energies as low as 0.3 eV, and (ii) the SPs dominate over bulk excitation even for large numbers of layers in a stack. In addition, we show that the SP energy is determined by the interplay between interband transitions and boundary effects. Given the large possibilities of engineering MXenes' electronic structure, this paper shows that, in principle, it is possible to directly tune the SP frequency in a large spectral range in the mid-infrared.

II. EXPERIMENTAL AND COMPUTATIONAL DETAILS

A. Experimental details

Samples were synthesized by etching the Al layers from Ti_3AlC_2 with hydrofluoric acid as described in Ref. [9]. For the EELS experiments, MXene powders were ultrasonicated in de-ionized water, and a drop of the solution was deposited on a holey carbon Cu grid. The spectra were acquired in a FEI Titan microscope, fitted with a monochromator and a high-resolution Gatan GIF Tridiem (Model 865) spectrometer. The spectra were acquired in STEM mode at 80 kV with the

*Vincent.mauchamp@univ-poitiers.fr

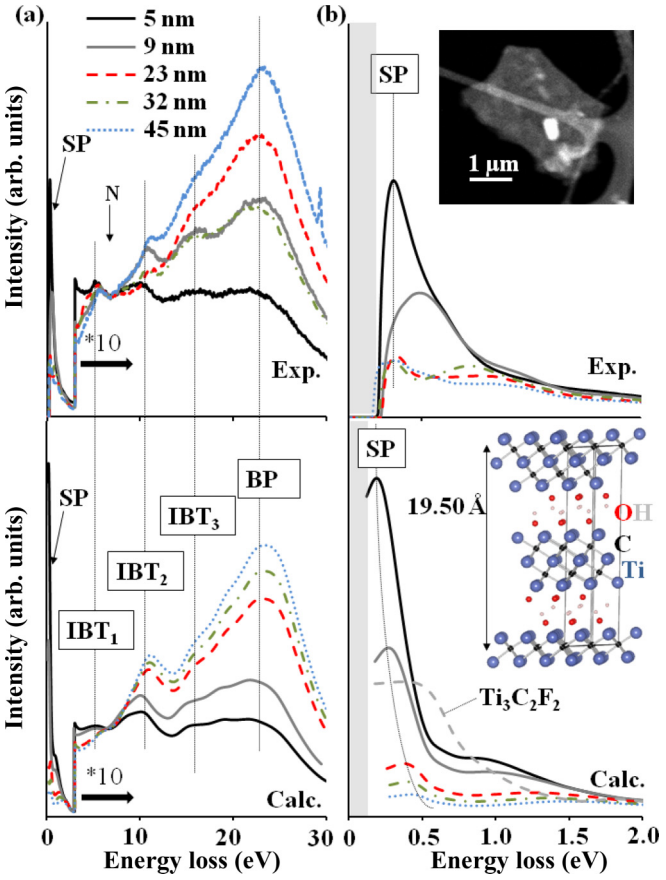

FIG. 1. (Color online) (a) Comparison between (top) the experimental and (bottom) the calculated—OH-terminated—low-loss spectra recorded on $Ti_3C_2T_2$ for different thicknesses. The spectra are normalized at 7 eV (labeled N) and are magnified by a factor of 10 above 3 eV. (b) Detailed view of the surface plasmon energy region. Insets: (Top) typical STEM–annular dark-field image of the samples and (bottom) $Ti_3C_2(OH)_2$ unit cell used for the calculations.

monochromator excited to allow for an energy resolution better than 0.1 eV at full width at half maximum (FWHM) of the elastic peak. In order to access the surface plasmons down to the infrared regime, the extraction of the inelastic contribution was performed using a Richardson-Lucy deconvolution scheme following the description of Bellido *et al.* [21]. The sample thicknesses were estimated from the low-loss spectra using the log-ratio technique [22]. Such a method was shown to give an accuracy on the order of 10% to 20% of the actual thickness [23,24].

B. Computational details

Experimental results are interpreted using the MXene energy-dependent dielectric function obtained in the optical limit from density functional theory calculations. Since the samples were probed along the [001] zone axis, the EEL spectra are determined by the in-plane dielectric response of the MXene $\varepsilon_{xx}(\mathbf{0},\omega)$ as already demonstrated in the case of the MAX phases [25,26]. The theoretical EEL spectra are computed in a semiclassical framework using the electron inelastic-scattering probability determined by Kröger for thin films in normal incidence [27]: Given that $\varepsilon_{xx}(\mathbf{0},\omega)$ is obtained from *ab initio* calculations, there are no adjustable parameters in our model.

$\varepsilon_{xx}(\mathbf{0},\omega)$ was computed with the WIEN2K code, an all electron full potential approach based on an augmented plane-wave formalism including local orbitals [28,29]. Because the hydrogen atoms are described with very small muffin-tin radii, the plane-wave basis set expansion was converged for a $RK_{\max}$ value of 3.5 for OH-terminated $Ti_3C_2T_2$. For $Ti_3C_2F_2$, a $RK_{\max}$ value of 7.5 was used. Since many-body effects were shown to be negligible in the basal plane dielectric response of the *MAX* phases [25,26], the present calculations were performed in the independent particle approximation using the OPTIC package of WIEN2K [30]. Exchange and correlation effects were treated in the generalized gradient approximation (GGA) (Perdew-Burke-Ernzerhof (PBE) parametrization [31]) which, for MXenes, gives results in very good agreement with hybrid functionals [12]. This approximation is well justified since GGA was shown to give an accurate description of the dielectric response of many metals including transition metals [32]. GGA has also been demonstrated to give a good description of *MAX* phases' plasmons [25,26], which gives strong support to the present calculations. $Ti_3C_2T_2$ exhibits a metallic behavior along its basal plane with a Drude frequency quite close to that of the parent Ti_3AlC_2 phase ($\hbar\omega_{p,xx}$ is 3.5 and 3.9 eV, respectively). Some $17\times17\times2$ and $27\times27\times3$ Monkhorst-Pack grids were used for the Brillouin zone sampling for the self-consistent field calculation of potentials and dielectric responses, respectively. The unit cells determined by complete geometry optimizations in Ref. [9] were used as input for the calculations. These structural models are expected to be fairly accurate since they give a good description of both the x-ray diffraction diagrams and the valence-band structure as probed by HREELS (see Fig. 1).

III. RESULTS AND DISCUSSION

A. Bulk plasmon

The experimental low-loss EEL spectra recorded on $Ti_3C_2T_2$ stacks of various thicknesses, ranging from 5 to 45 nm, are compared to the corresponding calculations (OH terminated) in Fig. 1(a). Given that the surface modes are much more intense than their bulk counterparts, intensities above 3 eV were magnified by a factor of 10. Based on these results, it is clear that the calculations reproduce well the energy positions of the interband transitions (IBTs) 1–3 and the bulk plasmon (BP). This point confirms that GGA is a reasonable approximation for the description of the basal plane dielectric response of $Ti_3C_2T_2$. The evolution of the relative intensities as a function of the thickness is also consistent between the calculations and the experiments. The BP intensity is significantly reduced as the MXene stack thickness is decreased, concomitantly the SP intensity significantly increases as evidenced in Fig. 1(b) where the corresponding energy range is magnified. We note however, that the experimental BP intensity of the 32-nm-thick sample is anomalously low. As detailed below, a slight disorder in the MXene stack could lead to such intensity reduction. The reduction in the bulk plasmon intensity is primarily due to

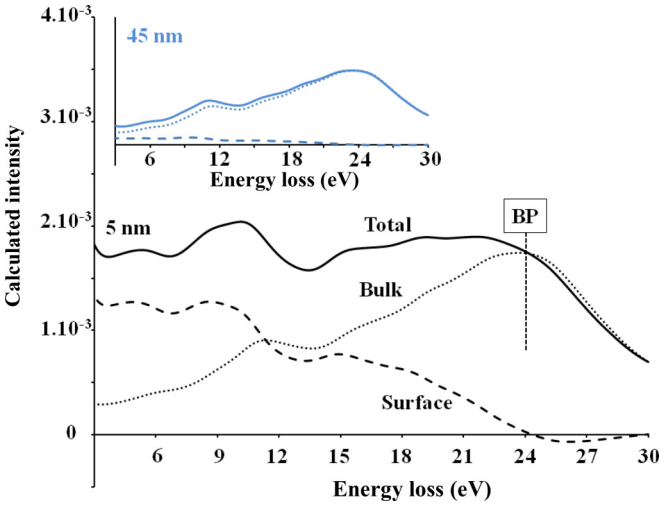

FIG. 2. (Color online) Surface (dashed line) and bulk (dotted line) contributions to the total (full line) cross section for a 5-nm-thick $Ti_3C_2T_2$ stack. Inset: Same quantities for a 45-nm-thick sample.

the important contribution of the surface terms in the total cross section at low thicknesses which, in addition to the SP, add a negative contribution at the bulk plasmon energy. This so-called begrenzungs effect is evidenced in Fig. 2 where the surface and bulk contributions to the total inelastic cross sections are given for the 5-nm-thick sample. In the inset, the surface and bulk contributions are also shown for the 45-nm-thick sample: The surface term is negligible in the bulk plasmon energy range, and the energy-loss spectrum is close to the bulk contribution.

As evidenced in Fig. 1, the bulk plasmon energy is insensitive to the number of MXene sheets: Given that a single MXene sheet is ≈1-nm thick [see the MXene unit cell in Fig. 1(b)], the BP energy remains unchanged when considering 5, 9, 23, 32, or 45 MXene sheets. This result is different from that observed in other 2D compounds, such as graphene, h-BN, or TMD where the bulk plasmon is blueshifted by several eV when going from few layers to bulklike systems [3,33–35]. Such plasmon shifts were interpreted on the basis that changing the stacking modifies the valence electron density involved in the screening, leading to a modification of the bulk plasmon energy [36]. This explanation is in line with the work of Marinopoulos *et al.* evidencing the shift in the $(\pi + \sigma)$ plasmon as a gauge of the intertube interaction in carbon nanotubes [37]. From these interpretations, the $Ti_3C_2T_2$ sheets appear as almost independent polarizable entities. We interpret this weak coupling between the $Ti_3C_2T_2$ sheets as a key feature accounting for their exceptional capacity to be intercalated with many different cations or small organic molecules [16,17].

B. Surface plasmon

The SP energy range is magnified in Fig. 1(b). For large thicknesses, the SP intensity decreases. This evolution is well reproduced by the calculations. We note that the SP energy position is slightly underestimated at 5 nm (ω_{SP}^{th}= 0.18 eV, ω_{SP}^{exp}= 0.28 eV) and progressively increases up to 0.42 eV at

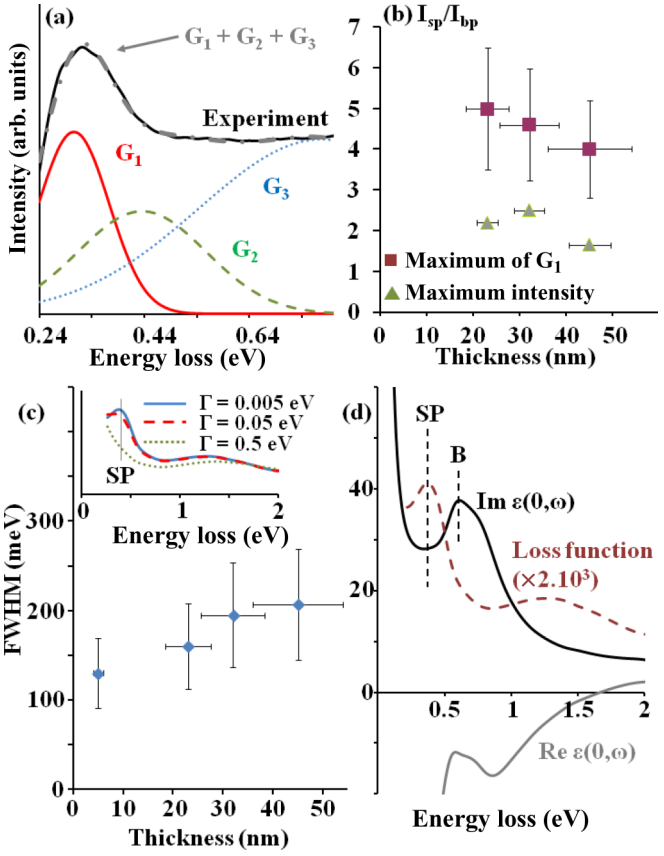

FIG. 3. (Color online) (a) Fit of the experimental SP with three Gaussians (G_1–G_3) for the 23-nm-thick sample. (b) Ratio of the SP to BP intensities determined either from the Gaussian fits or from the maximum intensities of the experimental spectra. (c) Full width at half maximum extracted from G_1 for the different thicknesses. Inset: Influence of the free-electron damping on the SP calculation. (d) Re $\varepsilon(\mathbf{0},\omega)$ and Im $\varepsilon(\mathbf{0},\omega)$ calculated for $Ti_3C_2(OH)_2$. The theoretical loss function for the 23-nm-thick MXene is also given for comparison.

45 nm whereas experimentally the SP energy remains constant. Moreover, one notices that the experimental SP of the 9-nm-thick sample is damped and blueshifted. This phenomenon can be understood from a theoretical point of view considering a F-terminated MXene model. The corresponding calculated low-loss spectrum is given in Fig. 1(b) (gray dashed lines). Compared to the OH-terminated model (full gray lines), the SP is clearly damped and blueshifted in agreement with the experimental results. Such a dependence of the SP on the MXene functionalization will be addressed in the next section.

Figure 1 highlights an important characteristic of the MXene's dielectric behavior: The SPs dominate over bulk ones even for a 45-nm-thick sample. The dependence of the SP characteristics (intensity, FWHM) on layer thickness was determined by fitting the experimental spectra with Gaussian functions as shown in Fig. 3(a). In the SP region (below 1 eV), three Gaussians were used. A typical result of such a fit is given in Fig. 3(a) for the 23-nm-thick sample: G_1 represents the surface plasmon around 0.3 eV, G_2 represents the maximum of the interband transitions around 0.5 eV [labeled B in Fig. 3(d)], and G_3 represents the interband excitations at higher energy. The same fitting procedure was applied to the bulk

plasmon region—between 13 and 30 eV—where here again three Gaussian functions were used for the IBT_3, the BP, and the background. The evolution of I_{SP}/I_{BP}, characterized by the ratios of the maxima of the corresponding Gaussians is shown in Fig. 3(b). Given its large damping, the SP of the 9-nm-thick sample (see Fig. 1) was disregarded here, and the values corresponding to the 5-nm-thick sample are not shown since they are one to two orders of magnitude larger. Unlike usually observed in transmission experiments, here the SPs dominate over the bulk ones at least up to 45-nm-thick samples. Similar results are obtained using the experimental maximum intensities of the EEL spectra [see Fig. 3(b)]. This behavior is peculiar: In gold or aluminum thin films, for instance, the SP vanishes for thicknesses greater than 30 nm [38,39].

This domination of surface modes can be traced back to the combination of three parameters. First, the screening dynamics of the free electrons in these systems is similar to that in plasmonic materials (Ag or Au). The SPs damping determined from their FWHM extracted from the fits presented in Fig. 3(a) is approximately 170 meV, a value very similar to that measured on Ag thin films [see Fig. 3(c)] [40]. This low SP damping, which arises from surface scattering, radiative, and nonradiative decays [5], goes together with a low free-electron damping. This is evidenced in the inset in Fig. 3(c) where the SPs calculated for different dampings—$\Gamma = 0.5$, 0.05, or 0.005 eV—in the Drude term of dielectric response are shown. Although it is not possible to precisely determine Γ by such comparisons, it is clear that it is on the order of 0.05 eV or less, a value very close to that reported for silver or gold [41]. The second point is that the SP energy is below the maximum of the interband threshold, labeled B in Fig. 3(d). It follows that the probability for the SP to decay into interband transitions is significantly reduced, a phenomenon shown to be crucial in other systems, such as gold nanorods [42]. Finally, the weak interactions between MXene sheets play a key role by reducing the bulk plasmon excitation probability. Indeed, plasmon wakes take place for thicknesses larger than $\lambda_p/4$ where λ_p is the plasmon wavelength [22,43]. For $Ti_3C_2T_2$, $\lambda_p \approx 30$ nm, a value that is much larger than the thickness of the individual sheets. $Ti_3C_2T_2$ thus fulfills the requirements of, and appears as, an alternative to what is currently attempted for graphene-based plasmonics where artificial heterostructures are fabricated to enhance their surface properties [39].

C. On the possibility to tune the surface-plasmon frequency

Regardless of sample thickness, the SP energy of $Ti_3C_2T_2$ is not determined by the simple condition $\mathrm{Re}\,\varepsilon(\omega) = -1$, which is fulfilled at 1.5 eV as evidenced from Fig. 3(d). To get a simple understanding of the SP dispersion relation as a function of the MXene thickness, we compare our results to those obtained assuming the nonretarded approximation for a Drude thin slab [5],

$$\omega_{SP}^{\pm} = \frac{\omega_p}{\sqrt{2}}[1 \pm \exp(-q_s t)]^{1/2}. \quad (1)$$

In Eq. (1), the + and − signs represent the antisymmetric and symmetric surface modes, respectively, and q_s is the SP wave vector. The evolution of ω_{SP}^{-} as a function of the MXene thickness t is calculated and is compared to both the experimental values and the *ab initio* calculations in Fig. 4. For the comparison, the free-electrons' plasma frequency used in Eq. (1) is taken from *ab initio* calculations [$\hbar\omega_p = 3.5$ eV for $Ti_3C_2(OH)_2$] and q_s from a free-electron model with a characteristic surface scattering angle of $\theta_s = \frac{\theta_E}{\sqrt{3}}$ (θ_E being the characteristic inelastic-scattering angle) [22]. The ω_{SP}^{+} is not considered since it falls within the interband continuum ($\omega_{SP}^{+} \approx 3$ eV) and is thus completely damped.

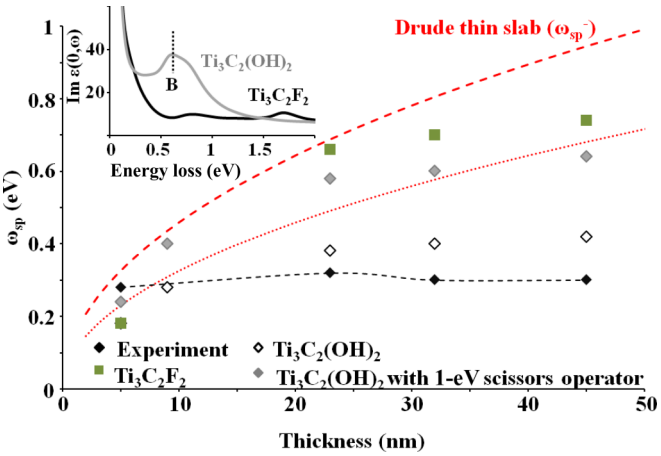

FIG. 4. (Color online) ω_{SP} as a function of the MXene thickness extracted from the experimental data (black diamonds) and the calculations: $Ti_3C_2(OH)_2$ (empty black diamonds), $Ti_3C_2(OH)_2$ considering a 1-eV scissors shift on the IBT (gray diamonds), $Ti_3C_2F_2$ (green squares), Drude thin slab model with q_s ($E = 0.3$ eV) (red dots), and q_s ($E = 0.6$ eV) (red dashed lines). Inset: $\mathrm{Im}\,\varepsilon(\mathbf{0},\omega)$ for $Ti_3C_2F_2$ and $Ti_3C_2(OH)_2$.

At $t = 5$ nm, the Drude model value is in good agreement with the experimental one (see Fig. 4). For larger thicknesses, the SP of $Ti_3C_2T_2$ deviates from the free-electron behavior: It is much less dependent on thickness. This effect is ascribed to the interband transitions that constrain the SP below 0.5 eV. As an illustration of the influence of the interband transitions on the SP, the loss function of $Ti_3C_2(OH)_2$ was calculated using a dielectric function where a 1-eV scissors operator was applied on the interband transitions, thereby blueshifting the interband threshold from the SP energy range. The SP frequency calculated using this new dielectric response was now free to increase from 0.2 to more than 0.6 eV for thicknesses ranging from 5 to 45 nm (gray diamonds in Fig. 4). These results clearly demonstrate that manipulating the MXene's electronic structure allows a complete tuning of the SP resonance, provided that the MXene's thickness is controlled. An obvious way of controlling the MXene's electronic structure is by changing its functionalization, e.g., substituting OH by F terminations. The evolution of ω_{SP} for the $Ti_3C_2F_2$ system is also shown as solid green squares in Fig. 4: The latter's response is close to that observed for $Ti_3C_2(OH)_2$ with a 1-eV scissors operator. The reason is that the interband maximum (peak B for OH-terminated MXenes) is shifted. As shown in the inset of Fig. 4, $\mathrm{Im}\,\varepsilon(\mathbf{0},\omega)$ behaves smoothly for $Ti_3C_2F_2$ in the 0–2-eV energy range. The SP is then free to obey the free-electron behavior, and the SP energy can be tuned from 0.18 to 0.74 eV for thicknesses ranging from 5 to 45 nm.

Given the weak interactions between the $Ti_3C_2(OH)_2$ sheets evidenced from their bulk plasmons and consistent with their high capacity to be intercalated easily by cations or molecules, manipulating the $Ti_3C_2(OH)_2$ thickness should be possible.

IV. CONCLUSION

To summarize, the dielectric properties of $Ti_3C_2T_2$ multilayers have been characterized combining high-resolution transmission EELS with *ab initio* calculations in the 0.2–30-eV energy range with special focus on the bulk and surface plasmons. The SPs have been evidenced at the nanometer scale and at very low energy in the mid-infrared, a spectral range of particular interest for chemical sensing [6]. The remarkable intensity and possible tunability of these SPs are discussed in terms of several factors that could be valid for other MXenes: (i) The screening dynamics of the free electrons are comparable to those in standard plasmonic materials. (ii) The MXene structure, built on weakly interacting 2D sheets, inherently reduces the probability of bulk excitations leaving surface modes as the dominant screening process. This weak interaction between MXene sheets is a key property for their outstanding capacity to be intercalated easily by a host of organic molecules and cations. (iii) The SP energy is shown to be determined by the interplay between electronic structure and boundary effects: Depending on the functionalization, the SP wavelength of $Ti_3C_2T_2$ can be kept constant or can be varied in a wide spectral range (from 6 to less than 2 μm for thicknesses ranging from 5 to 45 nm), these variations being controlled by the MXene thickness. This new class of 2D materials thus shows very promising behavior for surface plasmon-based applications since their SPs fulfill two major requirements: Tunability and enhancement thanks to their unique nanostructures.

ACKNOWLEDGMENTS

The authors thank Dr. M. Kurtoglu for his help concerning MXene structures and Professor Y. Gogotsi for his valuable comments on the paper. M.B., E.P.B., and G.A.B. are grateful to NSERC for the Discovery and Accelerator Grant supporting this work. The experimental work was carried out at the Canadian Center for Electron Microscopy, a national facility supported by NSERC and McMaster University. M.W.B. acknowledges the support of NSF Grant No. DMR-1310245.

[1] A. K. Geim, Science **324**, 1530 (2009).
[2] K. S. Novoselov, D. Jiang, F. Schedin T. J. Booth V. V. Khotkevich, S. V. Morozov, and A. K. Geim, Proc. Natl. Acad. Sci. U.S.A. **102**, 10451 (2005).
[3] J. N. Coleman, M. Lotya, A. O'Neill, S. D. Bergin, P. J. King, U. Khan, K. Young, A. Gaucher, S. De, R. J. Smith, I. V. Shvets, S. K. Arora, G. Stanton, H.-Y. Kim, K. Lee, G. T. Kim, G. S. Duesberg, T. Hallam, J. J. Boland, J. J. Wang, J. F. Donegan, J. C. Grunlan, G. Moriarty, A. Shmeliov, R. J. Nicholls, J. M. Perkins, E. M. Grieveson, K. Theuwissen, D. W. McComb, P. D. Nellist, and V. Nicolosi, Science **331**, 568 (2011).
[4] R. H. Ritchie, Phys. Rev. **106**, 874 (1957).
[5] H. Raether, *Surface Plasmons on Smooth and Rough Surfaces and on Gratings* (Springer-Verlag, Berlin, 1988).
[6] R. Stanley, Nat. Photon. **6**, 409 (2012).
[7] L. Ju, B. Geng, J. Horng, C. Girit, M. Martin, Z. Hao, H. A. Bechtel, X. Liang, A. Zettl, Y. R. Shen, and F. Wang, Nat. Nanotechnol. **6**, 630 (2011).
[8] H. Yan, T. Low, W. Zhu, M. Freitag, X. Li, F. Guinea, P. Avouris, and F. Xia, Nat. Photon. **7**, 394 (2013).
[9] M. Naguib, M. Kurtoglu, V. Presser, J. Lu, J. Niu, M. Heon, L. Hultman, Y. Gogotsi, and M. W. Barsoum, Adv. Mater. **23**, 4248 (2011).
[10] M. Naguib, O. Mashtalir, J. Carle, V. Presser, J. Lu, L. Hultman, Y. Gogotsi, and M. W. Barsoum, ACS Nano **6**, 1322 (2012).
[11] M. W. Barsoum, *MAX Phases: Properties of Machinable Ternary Carbides and Nitrides* (Wiley, VCH, 2013).
[12] Y. Xie and P. R. C. Kent, Phys. Rev. B **87**, 235441 (2013).
[13] A. N. Enyashin and A. L. Ivanovskii, Comput. Theor. Chem. **989**, 27 (2012).
[14] A. N. Enyashin and A. L. Ivanovskii, J. Solid State Chem. **207**, 42 (2013).
[15] M. Khazaei, M. Arai, T. Sasaki, C.-Y. Chung, N. S. Venkataramanan, M. Estili, Y. Sakka, and Y. Kawazoe, Adv. Funct. Mater. **23**, 2185 (2013).
[16] M. R. Lukatskaya, O. Mashtalir, C. E. Ren, Y. Dall'Agnese, P. Rozier, P. L. Taberna, M. Naguib, P. Simon, M. W. Barsoum, and Y. Gogotsi, Science **341**, 1502 (2013).
[17] O. Mashtalir, M. Naguib, V. N. Mochalin, Y. DallAgnese, M. Heon, M. W. Barsoum, and Y. Gogotsi, Nat. Commun. **4**, 1716 (2013).
[18] J. Halim, M. R. Lukatskaya, K. M. Cook, J. Lu, C. R. Smith, L.-Å. Näslund, S. J. May, L. Hultman, Y. Gogotsi, P. Eklund, and M. W. Barsoum, Chem. Mater. **26**, 2374 (2014).
[19] D. Rossouw and G. A. Botton, Phys. Rev. Lett. **110**, 066801 (2013).
[20] O. Nicoletti, F. de la Peña, R. K. Leary, D. J. Holland, C. Ducati, and P. A. Midgley, Nature (London) **502**, 80 (2013).
[21] E. P. Bellido, D. Rossouw, and G. A. Botton, Microsc. Microanal., doi:10.1017/S1431927614000609 (2014).
[22] R. F. Egerton, Rep. Prog. Phys. **72**, 016502 (2009).
[23] H.-R. Zhang, R. F. Egerton, and M. Malak, Micron **43**, 8 (2012).
[24] T. Malis, S. C. Cheng, and R. F. Egerton, J. Electron Microsc. Tech. **8**, 193 (1988).
[25] V. Mauchamp, M. Bugnet, P. Chartier, T. Cabioc'h, M. Jaouen, J. Vinson, K. Jorissen, and J. J. Rehr, Phys. Rev. B **86**, 125109 (2012).
[26] V. Mauchamp, G. Hug, M. Bugnet, T. Cabioch, and M. Jaouen, Phys. Rev. B **81**, 035109 (2010).
[27] E. Kröger, Z. Physik **235**, 403 (1970).
[28] P. Blaha, K. Schwarz, G. K. H. Madsen, D. Kvasnicka, and J. Luitz, WIEN2K, *an Augmented Plane-Wave + Local Orbitals Program for Calculating Crystal Properties* (Karlheinz Schwarz, Techn. Universität Wien, Austria, 2001).

[29] G. K. H. Madsen, P. Blaha, K. Schwarz, E. Sjöstedt, and L. Nordström, Phys. Rev. B **64**, 195134 (2001).
[30] C. Ambrosch-Draxl and J. O. Sofo, Comput. Phys. Commun. **175**, 1 (2006).
[31] J. P. Perdew, K. Burke, and M. Ernzerhof, Phys. Rev. Lett. **77**, 3865 (1996).
[32] W. S. M. Werner, K. Glantschnig, and C. Ambrosch-Draxl, J. Phys. Chem. Ref. Data **38**, 1013 (2009).
[33] T. Eberlein, U. Bangert, R. R. Nair, R. Jones, M. Gass, A. L. Bleloch, K. S. Novoselov, A. Geim, and P. R. Briddon, Phys. Rev. B **77**, 233406 (2008).
[34] C. T. Pan, R. R. Nair, U. Bangert, Q. Ramasse, R. Jalil, R. Zan, C. R. Seabourne, and A. J. Scott, Phys. Rev. B **85**, 045440 (2012).
[35] P. Johari and V. Shenoy, ACS Nano **5**, 5903 (2011).
[36] A. Kumar and P. K. Ahluwalia, Physica B **407**, 4627 (2012).
[37] A. G. Marinopoulos, L. Reining, A. Rubio, and N. Vast, Phys. Rev. Lett. **91**, 046402 (2003).
[38] H. Boersch, J. Geiger, A. Imbusch, and N. Niedrig, Phys. Lett. **22**, 146 (1966).
[39] L. Rast, T. J. Sullivan, and V. K. Tewary, Phys. Rev. B **87**, 045428 (2013).
[40] Y. Yu, Y. Jiang, Z. Tang, Q. Guo, J. Jia, Q. Xue, K. Wu, and E. Wang, Phys. Rev. B **72**, 205405 (2005).
[41] P. R. West, S. Ishii, G. V. Naik, N. K. Emani, V. M. Shalaev, and A. Boltasseva, Laser Photon. Rev. **4**, 795 (2010).
[42] C. Sönnichsen, T. Franzl, T. Wilk, G. von Plessen, J. Feldmann, O. Wilson, and P. Mulvaney, Phys. Rev. Lett. **88**, 077402 (2002).
[43] F. J. García de Abajo and P. M. Echenique, Phys. Rev. B **45**, 8771 (1992).